DESIGN AND ANALYSIS OF A NEW COMPLIANT MICROGRIPPER WITH TWO WORKING MODES

ZEKUI LYU , QINGSONG XU

Abstract. The microgripper plays an important role in the micro-assembly system, which directly contacts the target object. The working range of a normally open or normally closed gripper is limited. In this paper, a monolithic flexible microgripper with dual piezoelectric-actuation modes is presented, which combines the characteristics of normally open and normally closed grippers. It has the advantage of enhancing the adaptability of the gripper for grasping objects of different sizes. Different types of bridge mechanisms and parallelogram mechanisms are used in the displacement amplification structure of the gripper. Based on the kinematics model, the displacement magnification ratio of the gripper is analyzed. The crucial structural parameters affecting the magnification were selected to complete the structural optimization of the gripper. Then, the performance of the optimized gripper is verified by performing finite element analysis simulation study. Finally, a prototype microgripper is built and a series of experiments has been performed. The working stroke, natural frequency, and two working mode of the purposed microgripper have been tested and verified. The experimental results reveal that the designed gripper has a large clamping range (860.81 μm) and a sufficient-high natural frequency (401 Hz).

Key words: Microgripper, Flexible mechanism, optimization, normally open gripper, normally closed gripper.

1. INTRODUCTION

MEMS has many advantages, such as small size, low power consumption, and high integration, which are incomparable to traditional electromechanical systems [1]. The emergence of micro-assembly technology makes it possible to produce mass MEMS devices on micro/nano scales [2]. Microgripper, as the end-effector of the manipulator, is an important component of the micro-assembly system [3], [4]. The piezoelectric actuated microgripper is widely used because of its high resolution, fast response, and easy control [5], [6].

The piezoelectric-actuated microgripper can be divided into a normally open gripper and a normally closed gripper [7]. The working process of normally open gripper and normally closed gripper is shown in Fig. 1. If the initial jaw gap is larger than the clamping gap, the gripper is named normally open. The normally

Department of Electromechanical Engineering, Faculty of Science and Technology, University of Macau, Macau, China

Ro. J. Techn. Sci. – Appl. Mechanics, Vol. 67, N° 1, P. 79–96, Bucharest, 2022

open gripper is suitable for operating small objects, whose size is smaller than the gripping gap. When the object enters the tip gap, the clamps are gradually closed under the drive of the piezoelectric actuator (PEA). Finally, the target is confined between the two tips by means of shape closure. On the contrary, the working mode of the normally closed gripper is different. When the clamping target is relatively large, the clamping claws will first move to expand the clamping gap. After the gap is large enough to accommodate the target object, the actuating voltage is disconnected or reduced to form the clamping action. The clamping effect of the normally closed gripper makes full use of the inertia of the flexure hinge to recover the deformation.

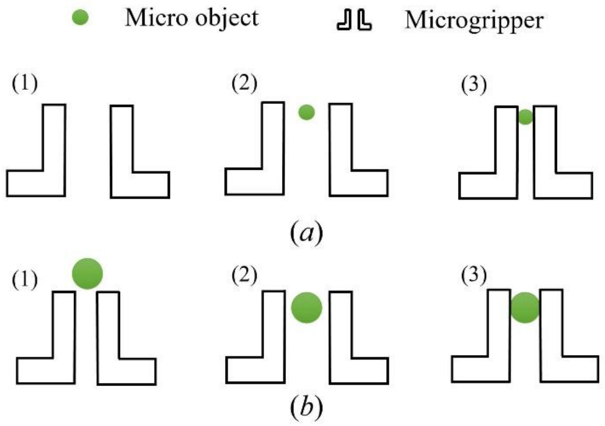

Fig. 1 – Sketch diagram of (*a*) normally open gripper and (*b*) normally closed gripper.

Numerous normally open grippers and normally closed grippers have been reported in the literature [8–16]. For example, Zubir et al. has presented a compliant normally open gripper for micromanipulation with a maximum stroke of 100 μm [8]. Wang et al. introduced a monolithic normally open clamp with displacement magnification of 16, which features parallel gripping and sensors integration [9]. In addition, Das et al. utilized a three-stage magnifying mechanism to design a normally open clamp, whose performance has been investigated for micro/nano-manipulation [10]. At present, the number of the normally closed gripper is far lower than that of the normally open gripper. Nah et al. have reported a normally closed compliant gripper using piezoelectric actuation, whose design, fabrication, and tests have been completed [14]. Kumar et al. have also purposed a normally closed clamp based on flexure-hinge and the parameters of the hinge have been studied and compared [15]. In addition, Choi et al. have developed a micromanipulation system, which has utilized a normally closed gripper [16].

Normally open grippers can be used to perform gripping operations when the size of the target is smaller than the gripper gap. In contrast, the normally closed gripper is suitable for the targets slightly larger than the gap. However, miniature targets often have different sizes in reality. This reduces the adaptability of the two grippers as mentioned above. One possible solution is the combination of a normally open gripper and a normally closed gripper. However, there is no gripper that combines normally open and normally closed characteristics in the literature.

In this paper, a new flexible gripper based on dual piezoelectric actuators is introduced, which has the advantages of the two operating modes as mentioned previously. The left side of the designed gripper is a normally open gripper and the right side is a normally closed gripper. The design, modeling, optimization, simulation, and experiment of the gripper are reported in detail in the following sections. The simulation and experimental results reveal that the optimized gripper has a dual working mode and remarkable gripping performance.

2. MECHANISM DESIGN AND MODELING

Fig. 2 provides the basic mechanical model of the designed microgripper, which is composed of the gripper body, two PEAs, two gaskets, and two preload screws. The geometric model of the gripper is constructed by the flexible hinges and rigid structure. Rectangular flexure hinges are used to generate and transfer deformation, which have the advantages of easy design, simple machining, and large deformation.

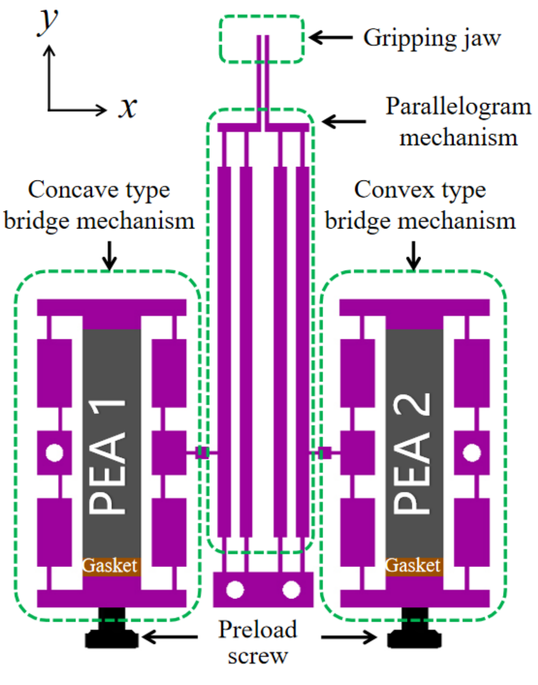

Fig. 2 – Schematic diagram of the proposed compliant microgripper.

The left and right sides of the gripper are made up of a two-stage displacement amplification mechanism, i.e., bridge-type mechanism and parallelogram mechanism. The levered parallelogram mechanism ensures the parallelism of grasp operation while carrying out displacement amplification.

It is worth noting that the right side of the gripper adopts a convex type of bridge mechanism, which will produce pulling force under the driving of PEA 2. The pulling force is transmitted to the parallelogram mechanism through the beam. The parallelogram mechanism is composed of two leverage mechanisms in parallel. It can reduce the parasitic movement while amplifying the desired displacement. In this case, the gripping jaw on the same side will move to the right to enlarge the gripping gap. On the contrary, the concave type of bridge mechanism is applied in the left clamp's structure to produce a pushing force. Similarly, the left gripping jaw will also be pushed to the right to shorten the jaw's gap. The benefit of this design is to improve the gripper's adaptability to the objects of different sizes, which will be described in more detail below. The preloading on the PEAs is implemented by tightening the preload screw on the back. At the same time, a gasket is placed between the PEAs and the preload screw to prevent undesirable rotation and damage of the PEAs. The overall gripper is designed as a monolithic structure, which reduces the errors during fabrication and assembly. The gripper can be installed on a precise motion platform through a fixed hole to achieve accurate movement.

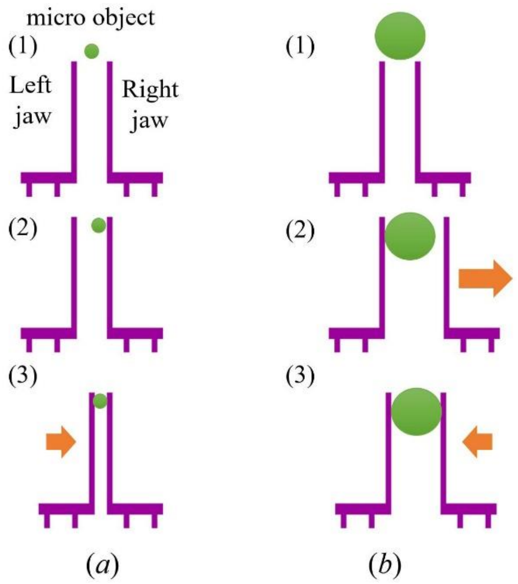

Fig. 3 – Two working modes of a gripper. (*a*) Normally open mode and (*b*) normally closed mode.

The proposed gripper has two clamping modes to improve the system's operational efficiency, as shown in Fig. 3. On the one hand, the PEA 1 will drive the left-side gripper to clamp the object when the size of the tiny target is smaller than the gripping gap. Fig. 3(a) shows the gripping process of this situation. On the other hand, the right-side gripper will be used when the size of the object is larger than the initial gap. In this case, the right jaw moves firstly to the right at a certain distance to make the gap cover the size of the object. Then, the voltage applied to PEA 2 will be gradually reduced to permit the tip to move back. The object entering the gripper gap will be clamped due to the elastic restorative force of the mechanism on the right, which is shown in Fig. 3(b).

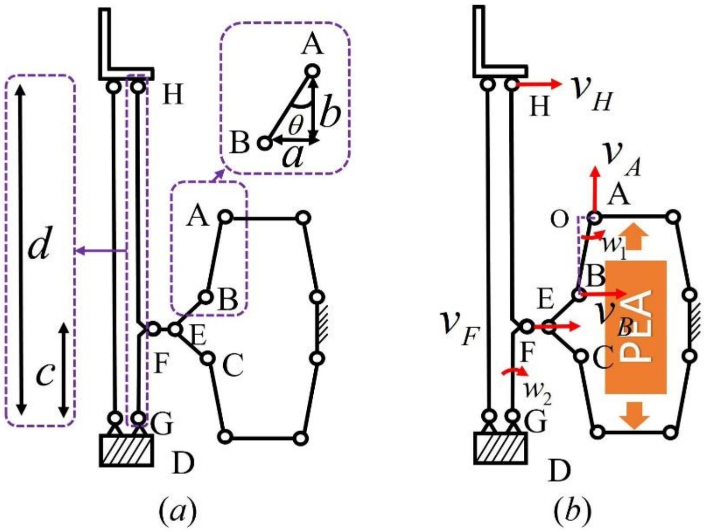

Fig. 4 – Simplified model of the gripper. (*a*) Pseudo-rigid-body model and (*b*) kinematic model.

The gripper's displacement magnification ratio (R_{amp}) is defined as the ratio of the output displacement (x_{out}) to the input displacement (x_{in}). To obtain the displacement magnification, a pseudo-rigid-body model (PRBM) for the flexible mechanism was established. The PRBM uses a rigid-body component with an equivalent force-deformation relationship to simulate the deformation of a flexible component. Considering the structural symmetry and similarity of the gripper's two sides, only the PRBM of the right-side gripper is presented here. Fig. 4(*a*) shows the PRBM and some critical geometric parameters of the right-side gripper. The magnification ratio is obtained from the instantaneous velocities at points A and H. The velocity vector diagram of the right gripper mechanism is shown in Fig. 4(*b*). The instantaneous center of the mechanism is determined by intersecting the vertical lines of the velocity directions at two different points on the linkage. Then, the instantaneous velocities at the points A, B, E, F, and H could be acquired, respectively. The relationships between them are shown as follows.

$$v_A = \omega_1 \cdot OA, \tag{1}$$

$$v_B = \omega_1 \cdot OB, \tag{2}$$

$$v_F = v_B, \tag{3}$$

$$v_F = \omega_2 \cdot \mathrm{FG}, \tag{4}$$

$$v_H = \omega_2 \cdot HG, \tag{5}$$

where ω_1 and ω_2 are the instantaneous angular velocities of the linkages AB and HF, respectively.

Based on the kinematic and geometrical relationships of the clamp, the displacement magnification ratio can be simply described as:

$$R_{amp} = \frac{x_{out}}{x_{in}} \cong \frac{v_F}{2v_A} = \frac{bd}{2ac} \tag{6}$$

According to the above equation, the jaw's motion position is linearly related to the actuating displacement. At the same time, it can be observed that the magnification is affected by the four mechanical parameters: *a*, *b*, *c*, and *d*, which are marked in Fig. 4(*a*). Based on this principle, the appropriate magnification can be obtained by adjusting the parameters of the corresponding flexible mechanism.

Similarly, the kinematics model of the left gripper can be analyzed in a similar way.

3. OPTIMIZATION OF STRUCTURE PARAMETERS

After completing the mechanism design of the gripper, the structural optimization design needs to be conducted to obtain the best performance. The goal of structural optimization design is to find the best design scheme according to a certain objective under the given constraint conditions.

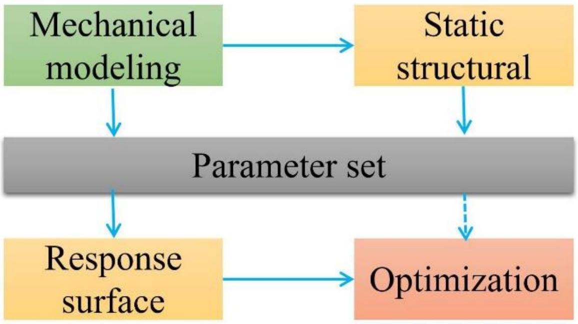

Fig. 5 –Schematic diagram of optimization design for the microgripper.

Design variables, objective functions, and constraints constitute a mathematical model for the optimal design of the microgripper. The optimization process is performed in commercial software ANSYS. The schematic diagram of optimization design is shown in Fig. 5. Firstly, suitable CAD software is selected to complete the mechanical modeling of the clamp. Then, the basic simulation is carried out in the static structural module. At the same time, the design variables (defined in the geometric model) and the objective functions (obtained in the static structural analysis) need to be imported into the parameter set. Indispensable constraints will be quantitatively described in the optimization module. Both direct optimization and response surface-based optimization can be used to achieve the design goals. Here, the response surface-based optimization is used to improve the performance of the gripper, as it can provide more detailed information.

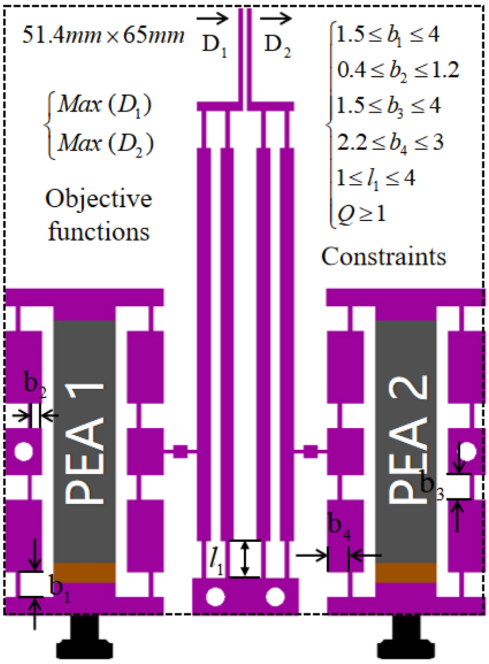

Fig. 6 – Illustration of the optimization model for the gripper.

Firstly, the end displacements (D_1 and D_2) of the clamping jaws on both sides are defined as the objective functions of the optimization model. The next step is to determine the structural variables to be optimized. The structure of the gripper has local symmetry, such as symmetric bridge and parallelogram mechanism. This arrangement can eliminate internal stress and reduce the complexity of the design. Hence, five structure parameters are assigned as the design variables, which have been selected to construct the optimization problem, as shown in Fig. 6. The parameters set [b_1, b_2, b_3, b_4] are related to the bridge mechanism, while the parameter l_1 influences the magnification of the leverage mechanism. The sensitivity curve based on ANSYS simulation result is shown in Fig. 7, which reflects the impact of each design variable on the optimization objective. From the curve, the deformation of the left tip is mainly based on the parameter set [b_1, b_2, l_1]. In addition, the parameter set [b_3, b_4, l_1] plays an important role in the deformation of the right gripper.

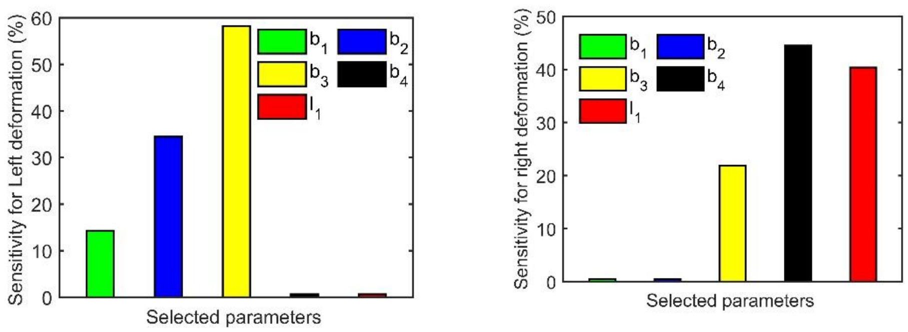

(*a*) (*b*)

Fig. 7 –Sensitivity analysis results based on ANSYS simulation. (*a*) Sensitivity for left-side deformation and (*b*) sensitivity for right-side deformation.

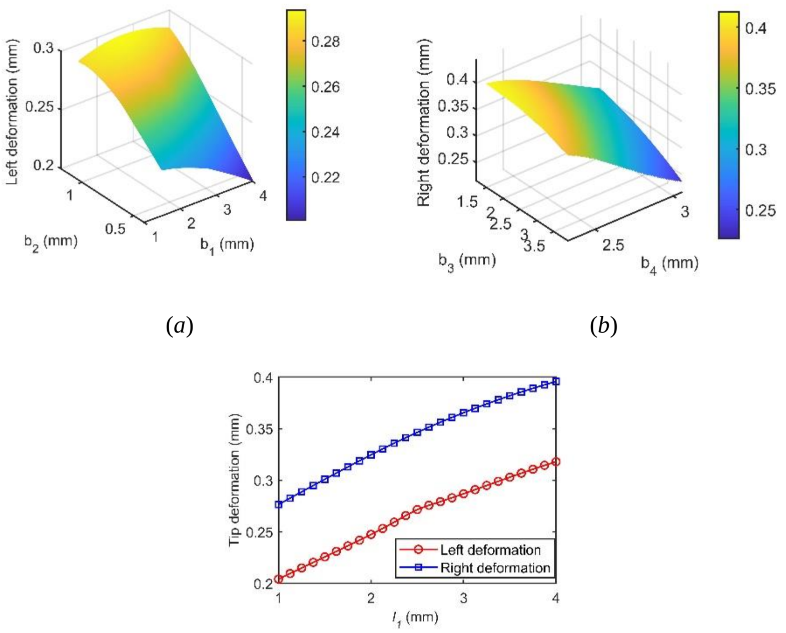

(*a*) (*b*)

(*c*)

Fig. 8 –Response surface and curve based on ANSYS simulation. (a) Response surface of b_1 and b_2 for D_1, (b) response surface of b_3 and b_4 for D_2, and (c) response curve of l_1 to the deformation of two sides for the gripper.

The effect of design variables on the objective function is observed through a response surface or response curve. In the response surface module, the response surface and response curve between the optimization target and the selected structural parameters are obtained, as shown in Fig. 8. From Fig. 8(a), the end deformation of the left gripper increases with the decrease of b_1 and the increase of b_2. The increase of b_3 and b_4 will result in a decrease in the right tip displacement as shown in Fig. 8(b). This difference is attributed to the inconsistency of the parameters in the optimization of the left and right bridge mechanisms. Fig. 8(c) displays the response curve of variable l_1 to the deformation of the gripper's two sides within the value range. There is an approximate direct proportional relationship between them. However, the deformation accuracy of longer rectangular flexure hinges will be reduced due to the lack of a rotation center. Therefore, the value of this variable should not be too large.

Obviously, it is a multi-objective optimization problem. Hence, the Multi-Objective Genetic Algorithm (MOGA) is used as an optimization algorithm because it supports multiple objectives and constraints. Furthermore, there is a physical constraint space (i.e., constraints) for each design variable. It is important to note that the safety factor (Q) of the whole mechanism should be greater than 1. Finally, the optimization model was converged after 1689 evaluations. Table 1 shows the constraints and final values for all the design variables.

Table 1

Constraints and final values of the optimized design variables.

Design variables	Lower limit	Upper limit	Optimum value
b_1 (mm)	1.5	4	2.6
b_2 (mm)	0.4	1.2	1.1
b_3 (mm)	1.5	4	2.6
b_4 (mm)	2.2	3	2.3
l_1 (mm)	1	4	4

4. FEA SIMULATION AND COMPARISON STUDY

To verify the reliability of the optimization results, it is necessary to carry out the performance simulation based on the finite element analysis (FEA). FEA utilizes mathematical approximations to simulate real physical systems to reduce engineering test costs. Here, the simulation environment chosen is the commercial ANSYS Workbench. The PEAs used here were substituted by a spring with the same stiffness. The preset mounting holes on the gripper are set as fixed support. The simulation study is primarily used to test the motion stroke and natural frequency of the gripper.

The working stroke of the gripper is simulated in the static structural module, which is shown in Fig. 9. The result in Fig. 9 reveals that the maximum deformation of the gripper occurs at the tip of the clamp. The maximum moving displacement of the left-side gripper is 345.56 μm while the maximum working stroke of the right-side gripper is 462.2 μm. Therefore, the displacement magnification of the left and right side gripper is 11.52 and 15.41, respectively. The amplification ratio obtained by the simulation is different from the theoretical calculation results (16.70 and 19.74). This discrepancy is induced because the in-plane thickness of the rectangular hinge is not considered. In addition, the PRBM is suitable for the analysis process of large-deformation compliant mechanisms, while the deformation magnitude of the gripper structure is small. In addition, the equivalent stress of the system is mainly distributed in the flexure hinge. The minimum safety factor of the structure is 6.0872, which is much higher than the assigned critical value of 1. The static performance analysis shows that the gripper can work normally without structural damage under the driving of PEA.

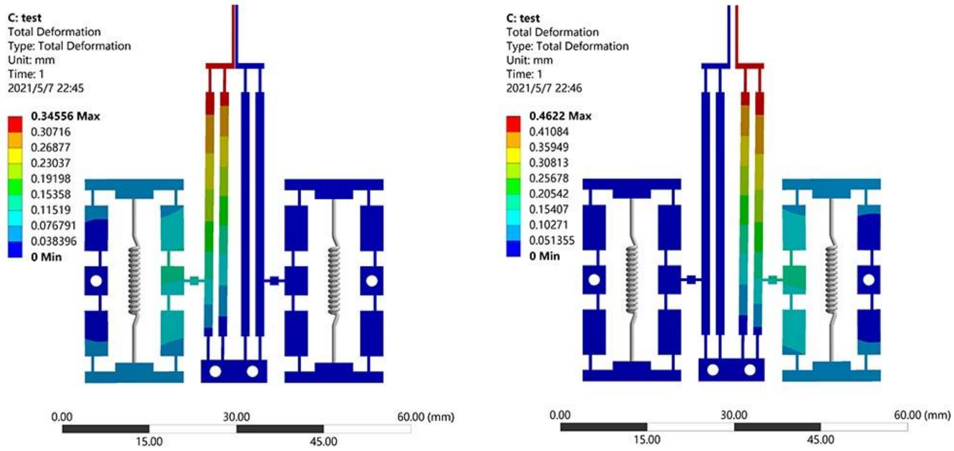

(*a*) (*b*)

Fig. 9 – Simulation results of (*a*) clamping stroke of the left-side gripper and (*b*) working stroke of the right-side gripper.

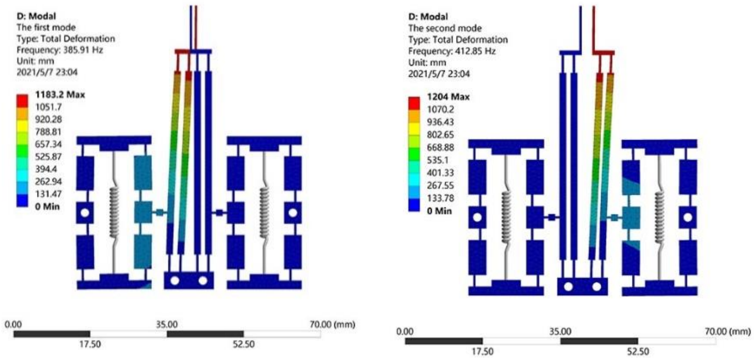

(*a*) (*b*)

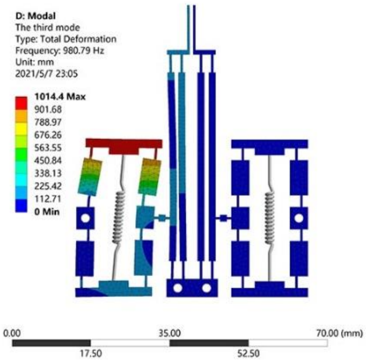

(*c*)

Fig. 10 – Simulation results of the first-three modal shapes of the microgripper. (*a*) The 1st natural frequency, (*b*) the 2nd natural frequency, and (*c*) the 3rd natural frequency.

Natural frequency is an important parameter to characterize the dynamic performance of the gripper, which is simulated with the modal module. Fig. 10 depicts the first three modes of the gripper and their corresponding natural frequencies. The first mode corresponds to the working mode of the left-side gripper, and its natural frequency is 385.91 Hz. Similarly, the natural frequency of the second mode is 412.85 Hz, which is the working mode of the right-side gripper. It is observed that the working frequencies of the two sides of the gripper were close to each other. In addition, the third mode of the gripper is contributed by the left bridge mechanism, which rotates clockwise around the plane with a frequency of 1014.4 Hz. Therefore, the simulation results show that the designed gripper has good dynamic performance.

5. EXPERIMENTAL TESTS

A prototype of the designed microgripper has been fabricated with the technology of wire electro-discharge machining (WEDM), as shown in Fig. 11(*a*). This processing technology has the advantages of integrated forming and high precision. The overall structure size of the gripper is 51.4 mm × 65 mm × 5 mm. The width of the rectangular flexure hinge is designed to be 0.5 mm due to the limitations of machining technology. The gap distance between the two jaws is set as 400 μm, which can be adjusted by the preloaded bolt. The material selected for manufacture is Al-7075 because of its outstanding mechanical properties. The fully assembled clamp is displayed in Fig. 11(*b*), which is consistent with the concept design in Fig. 1. The gripper is fixed on a base or a connector which is used to mount onto other devices, e.g., a micropositioning stage. In addition, the PEA model is RP150/5×5/30. It has a nominal displacement of 30 μm with an output thrust of 900 N.

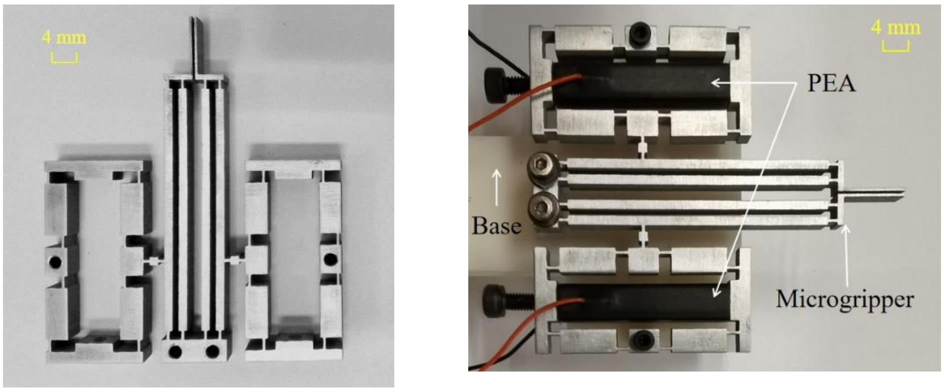

(*a*) (*b*)

Fig. 11 –Photo of the fabricated gripper prototype. (*a*) Planar microgripper mechanism and (*b*) assembled microgripper.

To examine the capability of the clamp, the experimental apparatus setup has been built. Fig. 12 displays the schematic diagram of the experimental setup and the photo of the physical apparatus. The microgripper is connected to an XYZ displacement platform (model: HTCL25-X, from Newport Corp) through a base. The displacement platform ensures that the gripper has a 3D space movement ability. Two laser sensors (model: LK-H055, from Keyence Corp.) are used to monitor the tension stroke of the gripper tip. The measurement range can reach ± 10 mm. The signal collected by the laser sensor is transmitted to the master computer through the NI 9215 module. The NI 9263 module and voltage amplifier (model: EPA-104, from Piezo Systems, Inc.) are adopted to provide input voltage for PEA. Both the NI 9215 and NI 9263 modules are mounted in slots in a reconfigurable embedded case connected to a real-time controller (model: NI cRIO 9022, from National Instruments Corp.). At the same time, two industrial cameras (model: MV-CE013-80UM, from Hikvision Corp.) were used to monitor the movement of the end of the clamp to provide more detail. All devices are mounted on a vibration isolation table (model: RS2000, from Newport Corp.).

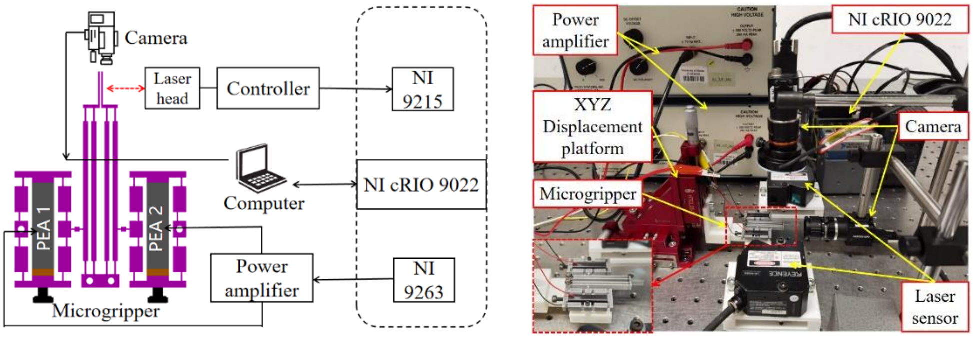

(*a*) (*b*)

Fig. 12 – Experimental setup for the microgripper. (*a*) Schematic diagram of the experimental setup and (*b*) photo of the experimental apparatus.

The open-loop experiments were carried out to test the gripping stroke and natural frequency of the clamp. Considering the separability of the actuator and structure on the left and right sides of the gripper, the above experiments were carried out twice. Detailed experimental results are given below.

Fig. 13 shows the gripping performance of the gripper under the driving of full-scale voltage. Specifically, Fig. 13(*a*)~(*c*) exhibits the test results for the left gripper, including the output actuating voltage, tip output displacement, and displacement hysteresis. Moreover, Fig. 13(*d*)~(*f*) shows the experimental results corresponding to the right gripper. The PEAs on the left and right sides are both driven by the voltage ranging from 0 to 150 V. When the actuating voltage is 150 V, the maximum stroke of the left gripper is 342.68 μm and the maximum stroke of the right gripper is 460.81 μm. So, the gripping range of the gripper lies in the range from 57.32 μm to 860.81 μm if the clamp clearance is 400 μm. This is consistent with the above-mentioned simulation results. In fact, closer results can be obtained by adjusting the preload bolt. The output displacement on both sides is approximately linear with the driving voltage. However, their output displacements are hysteretic. The maximum hysteresis errors on the two sides are 83.49 μm and 110.90 μm, respectively. This is caused by the hysteresis characteristic of PEA, and an appropriate control algorithm can reduce this error to improve the gripping accuracy.

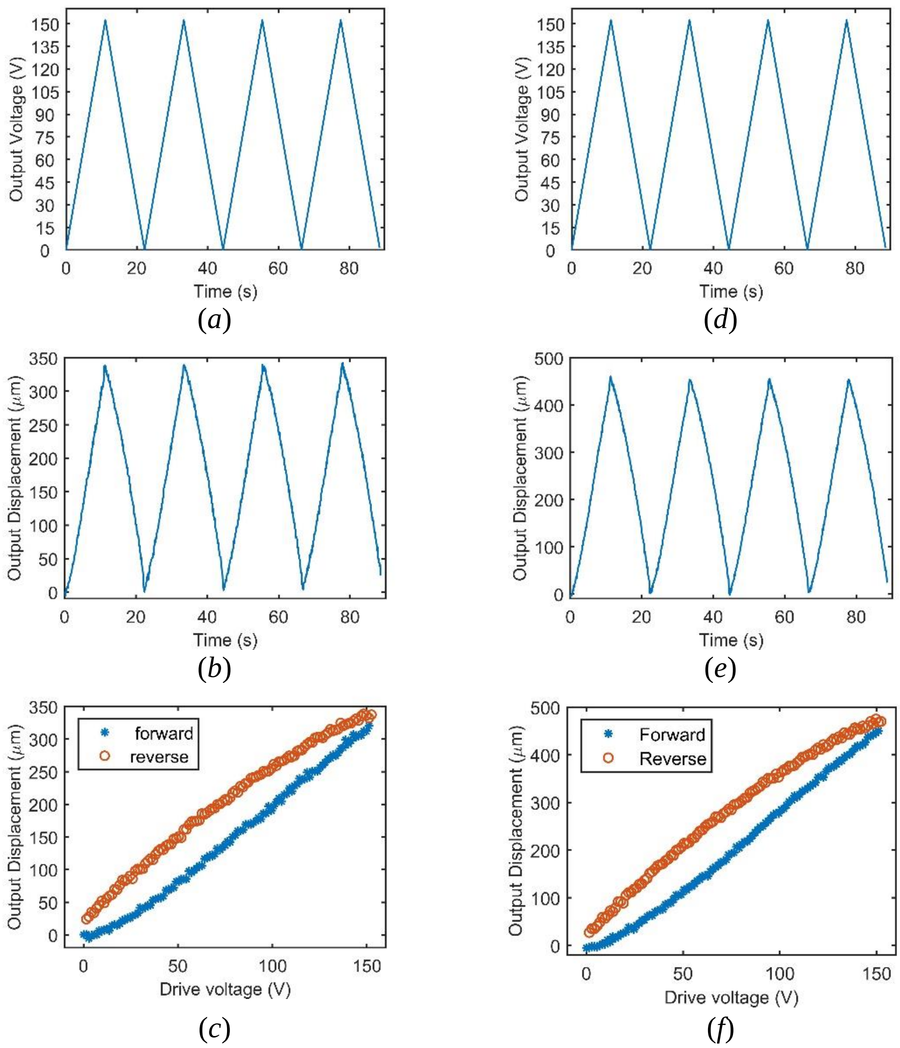

Fig. 13 – Experimental results of gripping displacement test. (*a*) Output voltage of power amplifier, (*b*) output displacement of the left tip, (*c*) hysteresis loop for the left tip, (*d*) output voltage of power amplifier, (*e*) output displacement of the right tip, and (*f*) hysteresis loop for right tip.

Frequency response test experiments were conducted on both two sides of the microgripper according to the results of the simulation. Specifically, sine waves with an amplitude of 4 V and frequency range of 1~500 Hz is produced to drive the PEAs. The gripper tip’s vibration was measured by the laser displacement sensors. When the resonance occurs, the tip of the gripper will produce violent shaking accompanied by harsh noise. By simple signal processing, the spectrum of the left and right grippers can be obtained, as shown in Fig. 14. The results show that the working vibration modes are excited, and the corresponding frequencies are 401 Hz and 398 Hz, which are close to the results of FEA simulation (385.91 Hz and 412.85 Hz). The discrepancy between them mainly arises from the added mass of other accessories and fabrication errors of the prototype.

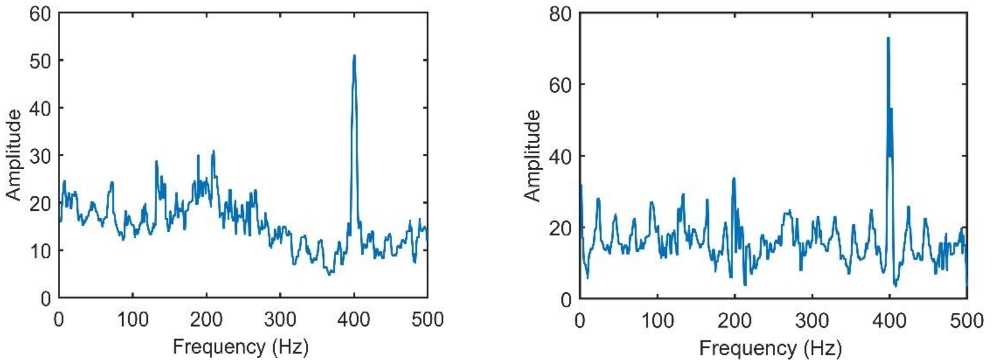

(*a*) (*b*)

Fig. 14 –Spectrum of the dynamic test result by experiment. (*a*) Left side and (*b*) right side.

To verify the applicability of the gripper, several grasping experiments have been carried out. For the objects whose size is smaller than the clamp gap, the gripper can be operated in normally open mode. When they enter the jaws, sufficient voltage is applied to the PEA 1 to achieve target gripping. The gripping process is shown in Fig. 15, where a micro-wire with the diameter of 300 μm has been gradually grasped. Fig. 15(*d*) displays the aluminum wire has been successfully grasped and held on in the air. In addition, the normally closed mode of the designed gripper has also been verified. In this situation, a solder wire with a diameter of 620 μm was selected as testing object, whose size is larger than the clamp clearance as shown in Fig. 16(*a*). Hence, the right PEA needs to be applied with appropriate voltage to open the clamp clearance. After that, the solder wire could be turned into the gap, as shown in Fig. 16(*b*). Next, the voltage to driven PEA 2 was gradually reduced to make the right jaw restore to its original position or a suitable position. In Fig. 16(*c*) and (*d*), the solder wire was precisely grasped and manipulated. Therefore, the proposed gripper has two working modes, i.e., normally open mode and normally close mode, and they both could operate successfully, which enhances the adaptability of the gripper to the clamping target size. The operator could select different working modes to grasp tiny objects according to their dimensions. This design reduces the time required to change the clamp and ensures the flexibility and consistency of the micromanipulation.

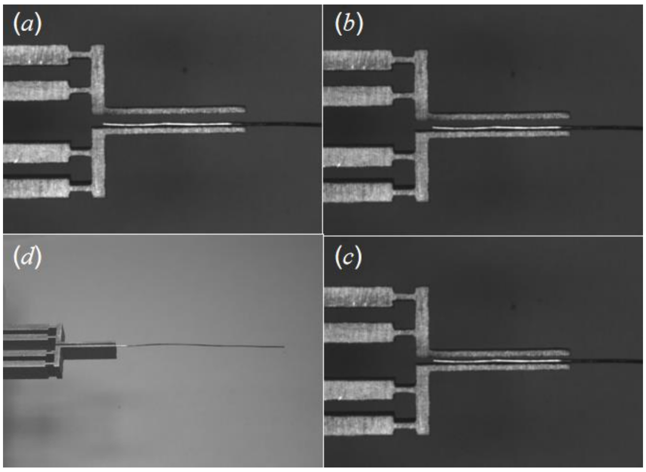

Fig. 15 –Gripping process of a wire with the diameter of 300 μm under normally open mode. (*a*) Wire enters clamp gap, (*b*) gradually grasping, (*c*) completely clamped, and (*d*) holding up.

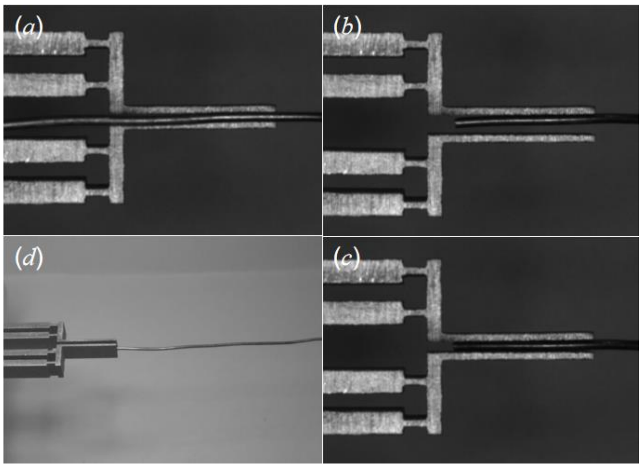

Fig. 16 –Gripping process of a wire with a diameter of 620 μm under normally close mode. (*a*) The wire diameter is greater than the clamp clearance, (*b*) wire enters the clearance after opening, (*c*) the right claw is gradually restored to its position, and (*d*) successfully grasping and holding up.

The performance comparison of typical piezoelectric actuated compliant microgrippers is exhibited in Table 2. Most grippers have only one operation mode, i.e., normally open or normally closed. As compared with other work, the proposed gripper has the advantages of double working modes and large clamping stroke. For the applications where the gripping target size is variable, the presented gripper will reduce the time consumed for adjusting or replacing the gripper.

Table 2

Performance comparison of typical microgrippers actuated by PEA.

Reference	Working mode	No. of amplification	Gripping stroke (μm)	First natural frequency (Hz)
[8]	Normally open	Two	100	-
[9]	Normally open	Two	432	-
[10]	Normally open	Three	93.52	1044
[13]	Normally closed	Two	180	-
[14]	Normally closed	Two	170	-
This work	Both	Two	803.49	401

5. CONCLUSION

This paper presents a new flexible gripper based on dual piezoelectric actuators. It is characterized by the combination of two working modes of normally open and normally closed. The proposed gripper has good adaptability to the size of the clamping target. Thus, the tiny target can be either smaller or slightly larger than the gripper gap. The operator can select the working mode according to the size of the target, avoiding the time wasted on adjusting or replacing the clamp. A two-stage flexible amplification mechanism is used on both sides of the gripper. Based on the PRBM, the kinematics model of the gripper is established, and the displacement magnification ratio is calculated. The geometric parameters related to the working stroke of the gripper were optimized by the MOGA. The working stroke and modal test of the gripper are verified with simulation and physical experiments. The working strokes of the left and right sides of the gripper are 342.68 μm and 460.81 μm, respectively. In addition, the first two natural frequencies corresponding to the operating modes of the gripper are 401 Hz and 398 Hz, respectively. Two different working modes of the gripper are successfully verified for metal wire with different diameters. Future work will focus on the precise control of the developed gripper. Displacement and force sensing and control will be considered to improve the reliability and precision of the gripper.

Acknowledgements. The authors gratefully acknowledge The Science and Technology Development Fund, Macau SAR (File no. 0153/2019/A3, 0022/2019/AKP, and 179/2017/A3), and University of Macau (File no. MYRG2018-00034-FST and MYRG2019-00133-FST).

Received on August 9, 2021

REFERENCES

1. MISHRA, M., DUBEY, V., MISHRA, P., KHAN, I., *MEMS technology: A review*, Journal of Engineering Research and Reports, **4**, *1*, pp. 1–24, 2019.
2. DEGTIARYOV, N., SUKHANOV, A., SUKHANOV, V., ARTEMOVA, A., FIRSOV, A., *Design and manufacture of miniature power microassemblies using 3d integration technology*, in Proc. of 2021 IEEE Conference of Russian Young Researchers in Electrical and Electronic Engineering, St. Petersburg and Moscow Russia, January pp. 26–28, 2021.
3. XU, Q., Design, *Fabrication and testing of an MEMS microgripper with dual-axis force sensor*, IEEE Sensors Journal, **15**, *10*, pp. 6017–6026, 2015.
4. YANG, S., XU, Q., NAN, Z., *Design and development of a dual axis force sensing MEMS microgripper*, Journal of Mechanisms and Robotics, Transactions of the ASME, **9**, *6*, p. 061011, 2017.
5. WANG, F., SHI, B., HUO, Z., TIAN, Y., ZHANG, D., *Control and dynamic releasing method of a piezoelectric actuated microgripper*, Precision Engineering, **68**, pp. 1–9, 2021.
6. XU, Q., *Robust impedance control of a compliant microgripper for high-speed position/force regulation*, IEEE Transactions on Industrial Electronics, **62**, *2*, pp. 1201–1209, 2014.
7. NIKOOBIN, A., NIAKI, M., *Deriving and analyzing the effective parameters in microgrippers performance*, Scientia Iranica, **19**, *6*, pp. 1554–1563, 2012.
8. ZUBIR, M., SHIRINZADEH, B., TIAN, Y., *A new design of piezoelectric driven compliant-based microgripper for micromanipulation*, Mechanism and Machine Theory, **44**, *12*, pp. 2248–2264, 2009.
9. WANG, D., YANG, Q., DONG, H., *A monolithic compliant piezoelectric driven microgripper: Design, modeling, and testing*, IEEE/ASME Transactions on Mechatronics, **18**, *1*, pp. 138–147, 2011.
10. DAS, T., SHIRINZADEH, B., GHAFARIAN, M., AL-JODAH, A., ZHONG, Y., SMITH, J., *Design, analysis and experimental investigations of a high precision flexure-based microgripper for micro/nano manipulation*, Mechatronics, **69**, p. 102396, 2020.
11. YANG, Y., WEI, Y., LOU, J., XIE, F., FU, L., *Development and precision position/force control of a new flexure-based microgripper*, Journal of Micromechanics and Microengineering, **26**, *1*, p. 015005, 2015.
12. SHI, Q., YU, Z., WANG, H., SUN, T., HUANG, Q., FUKUDA, T., *Development of a highly compact microgripper capable of online calibration for multisized microobject manipulation*, IEEE Transactions on Nanotechnology, **17**, *4*, pp. 657–661, 2018.
13. CHOI, H., LEE, D., KIM, S., HAN, C., *The development of a microgripper with a perturbation-based configuration design method*, Journal of Micromechanics and Microengineering, **15**, *6*, p. 1327, 2005.
14. NAH, S., ZHONG, Z., *A microgripper using piezoelectric actuation for micro-object manipulation*, Sensors and Actuators A: Physical, **133**, *1*, pp. 218–224, 2007.
15. RAGHAVENDRA, M., KUMAR, A., JAGDISH, B., *Design and analysis of flexure-hinge parameter in microgripper*, International Journal of Advanced Manufacturing Technology, **49**, *9-12*, pp. 1185–1193, 2010.
16. CHOI, H., SHIN, D., RYUH, Y., HAN, C., *Development of a micro manipulator using a microgripper and PZT actuator for microscopic operations*, in Proc. of 2011 IEEE International Conference on Robotics and Biomimetics, Karon Beach, Thailand, December 7-11, 2011.